**Forschungszentrum Karlsruhe**
in der Helmholtz-Gemeinschaft

**Wissenschaftliche Berichte**
FZKA 7060

# Thermal Hydraulic Analysis of Window Target Unit for LBE Cooled XADS

**N.I. Tak, H.-J. Neitzel, H.Y. Chen, X. Cheng**

**Institut für Kern- und Energietechnik**
**Programm Nukleare Sicherheitsforschung**

**Oktober 2004**

**Forschungszentrum Karlsruhe**

in der Helmholtz-Gemeinschaft

Wissenschaftliche Berichte

FZKA 7060

# Thermal Hydraulic Analysis of Window Target Unit for LBE Cooled XADS

N. I. Tak, H.-J. Neitzel, H. Y. Chen, X. Cheng

Institut für Kern- und Energietechnik

Programm Nukleare Sicherheitsforschung

Forschungszentrum Karlsruhe GmbH, Karlsruhe

2004

**Impressum der Print-Ausgabe:**

**Als Manuskript gedruckt**


**Forschungszentrum Karlsruhe GmbH**
**Postfach 3640, 76021 Karlsruhe**

**Mitglied der Hermann von Helmholtz-Gemeinschaft**
**Deutscher Forschungszentren (HGF)**

**ISSN 0947-8620**

**urn:nbn:de:0005-070609**

**Abstract**

Thermal Hydraulic Analysis of Window Target Unit for LBE Cooled XADS

A window target unit for a LBE cooled primary core is one of the basic options considered in the framework of the Preliminary Design Study of eXperimental Accelerator Driven System (PDS-XADS). In the present work, thermal hydraulic analysis has been performed for this option focusing on the window cooling. At first system analysis has been performed for the entire target unit using the one-dimensional system code, HERETA. Then Computational Fluid Dynamics (CFD) analysis has been carried out for lower part of the target to study the cooling capability of the window. The CFX 5.6 code has been applied using an advanced turbulence model, called Sheer Stress Transport (SST) model, combined with the advanced wall treatment available in the new CFX 5 version. The results of the HERETA calculations show that a stable natural circulation flow, with a steady state flow rate of 192 kg/s, is established. No temperature peak is observed by a start up procedure with beam ramp having a period of 200 s. It is found, however, a start up procedure with beam jump has to be avoided to prevent the overheating of the window. Based on the results of CFX 5.6 calculations, the window thickness is reduced to 2 mm in the center from the initial proposal of 3 mm in order to satisfy the thermal design limit. The maximum temperature change rate of the window under beam trips is predicted as high as 412 $^{o}$C/s after 0.1 s of the beam interrupt. It is judged that beam trips with a beam interrupt duration less than 1 s could also be crucial to the integrity of the window. Finally, three postulated accidents (i.e., beam focusing, loss of heat sink, and unexpected beam jump) have been analyzed to find out the time for the beam to be switched off in order to avoid window failure. The present results show that window failure occurs in 0.1~0.8 second after the start of the beam focusing and in about 200 seconds after loss of heat sink. However, window failure is not expected for a beam jump scenario during normal operation period with full reactor power.

**Kurzfassung**

Thermohydraulische Analyse der Fenster-Target-Einheit für das PbBi-gekühlte XADS

Eine Fenster-Target-Einheit für ein Blei-Wismut-gekühltes Primär-System ist eine der grundlegenden Optionen, welche im Rahmenprogramm der Preliminary Design Study of eXperimental Accelerator Driven System (PDS-XADS) untersucht wird. In der vorliegenden Arbeit ist für diese Option eine thermohydraulische Analyse insbesondere für die Fenster-Kühlung durchgeführt worden. Zunächst wurde eine System-Analyse für die gesamte Target-Enheit unter Verwendung des eindimensionalen System-Codes HERETA durchgeführt. Sodann wurde der untere Teil des Targets einer CFD-Analyse (Computational Fluid Dynamics analysis) unterzogen, um die Kühlbarkeit des Strahl-Fensters zu studieren. Dabei wurde der CFX 5.6 Code angewendet - unter Benutzung eines fortgeschrittenen Turbulenz-Modells, dem so genannten Sheer Stress Transport (SST) Modell, kombiniert mit den in der neuen CFX 5-Version verfügbaren fortentwickelten Wand-Funktionen. Die Ergebnisse der HERETA-Rechnungen zeigen, dass sich bei Einbeziehung einer Start-Prozedur mit einer Strahl-Leistungs-Rampe von 200 s Dauer eine stabile Natur-Konvektion mit einem Massenstrom von 192 kg/s einstellt. Mit einer solchen Prozedur ergeben sich keinerlei Temperatur-Überhöhungen. Es ist außerdem ermittelt worden, dass eine Start-Prozedur mit Strahl-Leistungs-Sprung vermieden werden muss, damit es zu keiner Überhitzung des Fensters kommt. Basierend auf CFX 5.6-Rechnungen muss die Wandstärke des Fensters in der axialen Mitte von den ursprünglich vorgeschlagenen 3 mm auf 2 mm reduziert werden, um die thermische Design-Grenze einzuhalten. Der maximale Temperaturanstieg im Fenster wurde bei Strahl-Unterbrechungen von 0.1 s Dauer zu 412 °C/s ermittelt. Es wird erwartet, dass auch Strahl-Unterbrechungen mit weniger als 1 s Dauer für die Integrität des Fensters kritisch sein könnten. Schließlich wurden drei angenommene Unfall-Szenarien (z.B. fokussierter Strahl, Verlust der Wärmesenke und unerwarteter Strahl-Sprung) analysiert, um die Zeit zu ermitteln, nach der der Strahl abgeschaltet werden muss, um ein Versagen des Fensters zu vermeiden. Die vorliegenden Ergebnisse zeigen, dass die entsprechenden Zeiten für ein Fenster-Versagen für zwei Unfall-Szenarien – fokussierter Strahl und Verlust der Wärmesenke – 0.1 bis 0.8 bzw. 200 Sekunden betragen. Hingegen ist bei einem plötzlichen Strahl-Sprung während des normalen Betriebes mit voller Reaktor-Leistung kein Fenster-Versagen zu erwarten.

**CONTENTS**

## 1. INTRODUCTION

Transmutation of long-lived radioactive-nuclides using an Accelerator-Driven System (ADS) is a promising solution for reducing the long-term radiotoxicity of nuclear wastes. The practicability of ADS of an industrial scale requires the operation of a small scale experimental ADS. One of the key milestones in the European ADS roadmap [1] is the design and construction of the European eXperimental ADS (XADS). At the present stage, European research institutions including Forschungszentrum Karlsruhe, industrial partners and universities are working together on the preliminary design study of the European experimental ADS (PDS-XADS project) under the 5$^{th}$ Framework Programme funded by the European Commission. The main objectives of the PDS-XADS project are to select the most promising technical options, to address the critical points of the entire ADS system (i.e., accelerator, spallation target unit, sub-critical core), to identify further research and development (R&D) needs and then, to consolidate the road map of the development of the European XADS [2].

Three different reactor core concepts are being taken into consideration, i.e., a small core (50 MW) cooled by lead-bismuth eutectic (LBE), a large (80 MW) LBE-cooled concept, and a large (80 MW) gas-cooled concept [2]. Related to the large core concepts, three different designs of spallation target have been investigated [3]. These are the window target in the LBE cooled core, the window target in the gas cooled core, and the windowless target in the LBE cooled core. There are some advantages and disadvantages in the window target compared to the windowless one. One of main challenges of the window target is the cooling capability of the window.

The window is a thin physical barrier to separate the vacuum from LBE. It is exposed to high thermal and irradiation loads, which affect its life time. The integrity of the beam window is crucial for a safe operation of ADS, preventing the penetration of the radioactive spallation products into the accelerator island. Therefore, a sufficient cooling capability of the beam window is one of the key issues of the target design.

The present report focuses on the thermal hydraulic analysis of the window target unit for the LBE cooled XADS core. It covers system analysis using a one-dimensional (1D) code as well as a CFD analysis. The system analysis was performed for the entire target unit, whereas the CFD analysis was carried out for the lower part of the target. A detailed simulation is required for the lower part of the target to get detailed results including the window temperature. The system analysis provides necessary boundary conditions for the CFD calculations. The CFX 5.6 code [4] is selected in the present work for the CFD analysis.

Steady state as well as transient behavior of the target unit in normal and off-normal

conditions has been investigated in the present study. In the steady state calculations, several parametric studies are also included to investigate the effects on the thermal hydraulic performance. In order to investigate transient behavior of the target, beam start up procedures (i.e., beam jump and beam ramp), beam interrupt transients, and three major accident scenarios (i.e., beam focusing, loss of heat sink, and unexpected beam jump) have been considered.

## 2. TARGET UNIT FOR LBE COOLED XADS

### 2.1 Description of Target

In the frame of the PDS-XADS project, feasibility studies on various options of the European experimental ADS are carried out. For the large LBE-cooled core concept, a pool type compact target module is proposed. Heat removal is based on naturally induced convection. Heat exchanger is integrated into the target module. The main advantages of this compact configuration are:

- Confinement of the spallation target into a well bounded small region;
- Inherent safe operation due to the purely natural convection operation mode;
- Simplicity of the target system.

The target unit is located in the center of the XADS core and consists of several co-axis cylinders. It is enclosed by the main shell which is the physical boundary between the spallation material (LBE) and the reactor coolant. Inside the main shell, there is an evacuated central beam tube. The mechanical design of the target is shown in Fig. 1. The total height of the target is 7.8 m. Since the LBE flow is driven by buoyancy force without pumps, a sufficient height and a small pressure loss are required to guarantee an efficient natural circulation.

The proton beam enters the beam tube at the upper end, penetrates the beam window and impinges on the upward flowing LBE. This produces a high thermal load to the window as well as LBE. About 70% of the beam energy is deposited as heat in the lower part. Therefore, detailed analysis using a CFD approach is necessary for this part. The rest of energy is contained in the particles escaping the target unit or in the binding energy of the nucleus of the spallation material. The deposited heat is removed in a heat exchanger at the upper end inside the target unit. Table 1 shows the main design parameters of the heat exchanger produced by the optimization analysis.

The guide tube is placed to separate the downward cold LBE and the upward hot LBE. The lower part of the guide tube is referred as funnel. A careful design of the funnel is important because it affects the natural circulation flow in the target and the injection flow to the window.

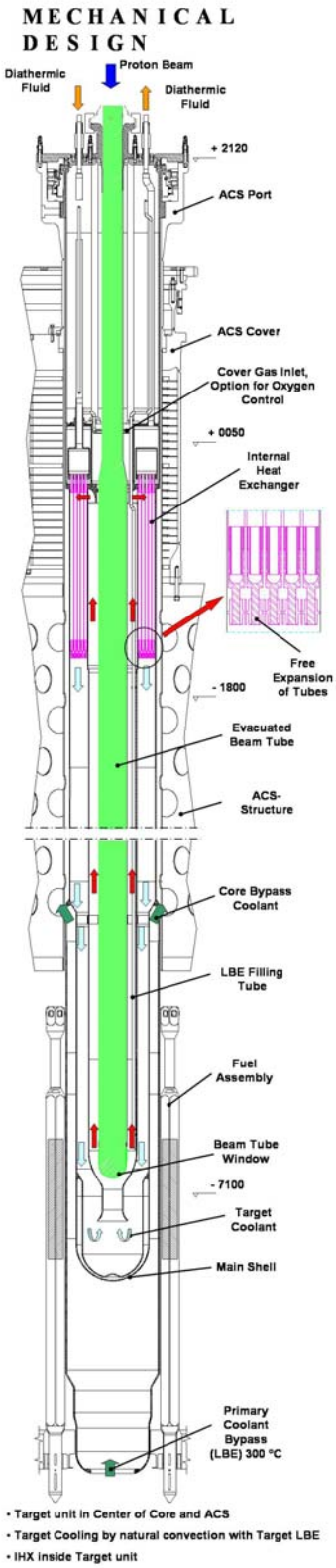


Fig. 1. Mechanical design of window target unit for LBE cooled XADS [5].

Table 1. Main design parameters of heat exchanger for XADS target [6]

| | |
|---|---|
| Height of heat exchanger | 840 mm |
| Number of tube ring | 5 |
| Number of tube | 308 |
| Type of tube | Double walled tubes |
| Diameter of outer tube | 21 mm |
| Diameter of inner tube | 15 mm |
| Wall thickness of tube | 1.5 mm |
| Tube pitch | 25 mm |

### 2.2 Thermal Hydraulic Design Limits

The design limits for the XADS target are defined in Ref. [7]. In the thermal hydraulic point of view, four design limits are adopted in the present work. These are:

(1) The maximum temperature of the beam window should be less than 525 °C.

(2) The maximum temperature of the window outer surface contacting LBE should not exceed 500 °C, to avoid a significant corrosion damage of the window. (In the present work, this limit is always satisfied when the limit criterion (1) is satisfied. Therefore the limit criterion (2) is neglected in the discussions.)

(3) The temperature limit for the other structural material such as the guide tube is 450 $^{o}$C. The temperature limit of the window is higher than that of the structural material because the life time of the window is shorter.

(4) The maximum local flow velocity of LBE should be less than 2 m/s, to minimize the erosion damage of the structural material.

### 2.3 Spallation Heat

The proton beam energy is 600 MeV. The footprint of the beam has a circular shape with the radius of 8 cm and the beam intensity follows an elliptical radial distribution as

$$\Phi(r) = \frac{3I_0}{2\pi r_0^2}\left[1-\left(\frac{r}{r_0}\right)^2\right]^{1/2} \qquad (1)$$

where $I_0$ is the total proton beam current, $r_0$ is the radius of the beam, and r is the radial distance from the axis of the beam. The heat deposition profile in the target unit was evaluated by Travleev and Broeders using the MCNPX 2.4.0 code. Their results are

summarized in Ref. [5] and [8]. In the MCNPX calculation fine meshes were adopted near the window to satisfy the CFD requirements. Figure 2 shows a contour plot for the heat deposition in the target unit. Line plots are provided in Figs. 3 & 4. As can be seen in Fig. 3, the maximum heat deposition density in the window reaches 0.14 kW/cm$^3$/mA on the center of the window outer surface, where flow stagnation is expected. As shown in Fig. 4, the maximum heat deposition density, 0.15 kW/cm$^3$/mA, is located ~2 cm below the window center.

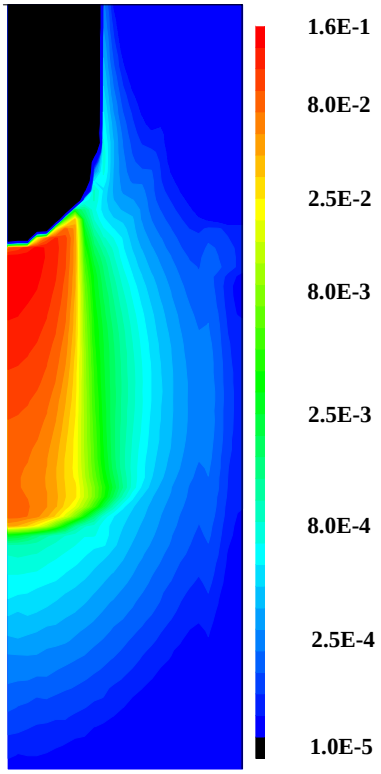


Fig. 2. Contour plot for heat deposition in the target (kW/cm$^3$/mA) [5].

During XADS operations, the beam intensity is increased with the fuel burnup to compensate the sub-criticality of the reactor core. In the present work, the maximum beam current (= 6 mA) from the XADS accelerator has been considered as the reference value for the target design. With 6 mA of the beam current, the total heat deposition in the entire target and in the window is 2.8 MW and 39 kW, respectively.

The neutronic calculation in Ref. [5] shows that during operation of a 1-batch-cycle of XADS the beam current varies from 2.47 mA at $k_{eff} \approx 0.97$ (typical for BOC) to 5.1 mA at $k_{eff} \approx 0.94$ (typical for EOC). It was found from this study that the heat deposition distribution near the reactor core is distorted with the change of the sub-criticality of the

reactor core. The total amount of heat deposition in the target is changed from 1.2 (483.1 kW/mA) to 2.4 MW (466.87 kW/mA) with the fuel burnup. However, the impact on the heat deposition distribution near the window and inside the funnel is very small.

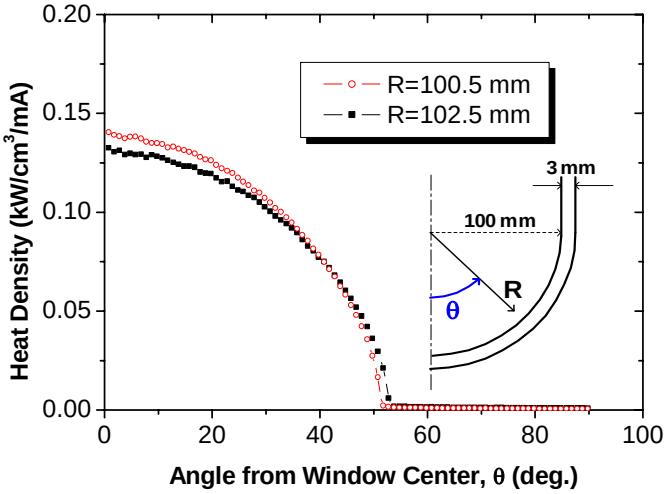


Fig. 3. Heat deposition distribution in the window [8].

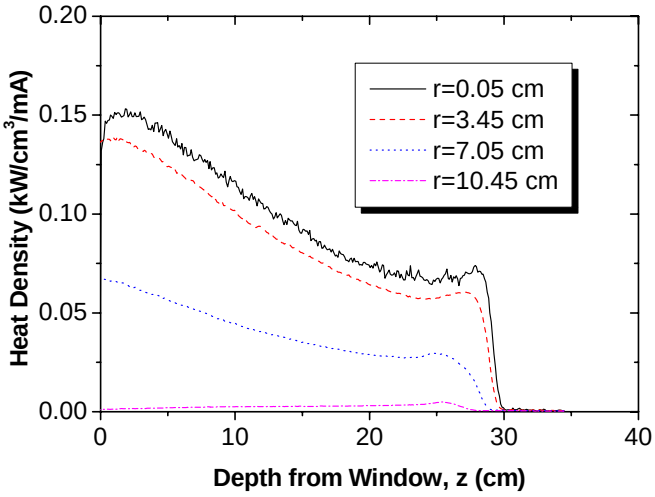


Fig. 4. Heat deposition distribution in LBE (r=0 at the beam axis) [8].

## 3. SYSTEM ANALYSIS WITH 1D CODES

### 3.1 Selection and Verification of Numerical Tools

#### 3.1.1 Available One-dimensional Codes

According to long experience, one-dimensional codes are considered as economic and powerful tools for design and analysis of nuclear components. For the system analysis of the XADS target unit, three different codes, i.e., HERETA, HETRAF, and RELAP-5, are available at Forschungszentrum Karlsruhe. The HERETA code was developed specifically for LBE cooled systems. It was applied to design of the large scale integral target test module K4T in KALLA. More details about the HERETA code can be found in [9]. The main features of the HERETA code are:

- Fluid-dynamic computer code for loops with natural convection driven flows
- Simulations of transient, one-dimensional, incompressible fluids with volumetric heat sources
- User subroutines for correlations of friction, heat transfer, and properties of materials
- Nodalization of loop: zones with 2 bounding surfaces and meshes.

The HETRAF code was originally developed for super-critical helium systems [10]. It was modified and extended to LBE systems. This code has been applied to the design analysis of the MEGAPIE target [11]. The main features of the HETRAF code are:

- Single phase flow
- Multi-loop system with thermal coupling
- Individual pump characteristics, control systems, and source terms
- Bypass loops
- Unlimited number of boundary coupling (thermal)

The LBE version of RELAP-5 was provided by ANSALDO [12]. This code has been applied for the safety analysis of XADS [13].

#### 3.1.2 Benchmark Exercise

For selection and verification of the computer codes for the present application, a benchmark exercise was carried out using these three codes.

*Reference Model for Benchmark*

For the benchmark purpose, a target system was defined, as illustrated in Fig. 5,

which is similar to the reference design proposal of the XADS target.

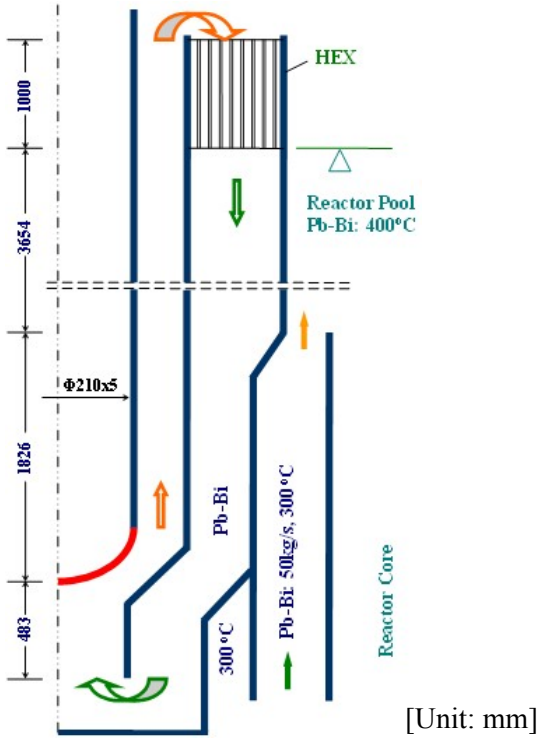


Fig. 5. Target configuration for benchmark exercise.

The heat exchanger configuration is the same as that of the XADS target module. Local hydraulic resistance was neglected, except at the entrance of the funnel and at the entrance of the heat exchanger. For both locations, a local pressure drop coefficient of 1.0 was taken. All three codes used the same properties for structural material (steel). The entire target module is divided into three regions according to axial elevations. In the lower part, the target is connected to the reactor core region. An overall uniform temperature of LBE in core (300°C) was assumed. In the middle part, the target is in connection with the upper part of the LBE pool, where the average LBE temperature is 400°C. The upper part of the target, i.e., the heat exchanger region, couples with the gas room above the LBE pool. The heat exchange between the target and the gas region was neglected. A total heat release of 2.63 MW in the spallation zone was used. 50% of the heat is deposited in the upper 100 mm depth of the spallation zone. The other 50% is uniformly distributed over the lower region of 383 mm. 20% of the total heat is released in the region outside the funnel. It was also assumed that no heat is directly released in the structural material. For both the HERETA and HETRAF codes, the same correlations of heat transfer, friction pressure drop and LBE properties were applied. Because only the executable version of RELAP-5 is available, the physical models and

LBE properties in RELAP-5 cannot be changed. A minor deviation of physical models and LBE properties might exist between HERETA and RELAP-5. Because RELAP-5 does not have the possibility to directly simulate heat source in fluid, a virtual solid material is introduced into the spallation zone, to simulate the spallation heat in the spallation zone. This virtual solid material was selected in such a way, that its effect on the transient behavior is minimized.

*Transient Scenario for Benchmark*

The following transient scenario was selected as benchmark case. Before the transient process starts, the entire system is at rest. The temperature of LBE and structural material is 300 °C. At the time point t=0 s, heat exchanger is activated. In the secondary side of the heat exchanger, oil flows into the heat exchanger at a temperature of 170 °C with a mass flow rate of 145 kg/s. At the time point t=500 s, the proton beam is switched on with its full power.

*Results of Benchmark*

Figure 6 shows the transient behavior of the LBE mass flow rate. The results from all three codes agree well with each other. Minor deviation is obtained between RELAP-5 and other two codes. RELAP-5 gives a little slower increase in the mass flow rate after the activation of oil flow, but a faster increase in the mass flow rate after the switch-on of the proton beam. It gives slightly lower mass flow rate at steady state conditions.

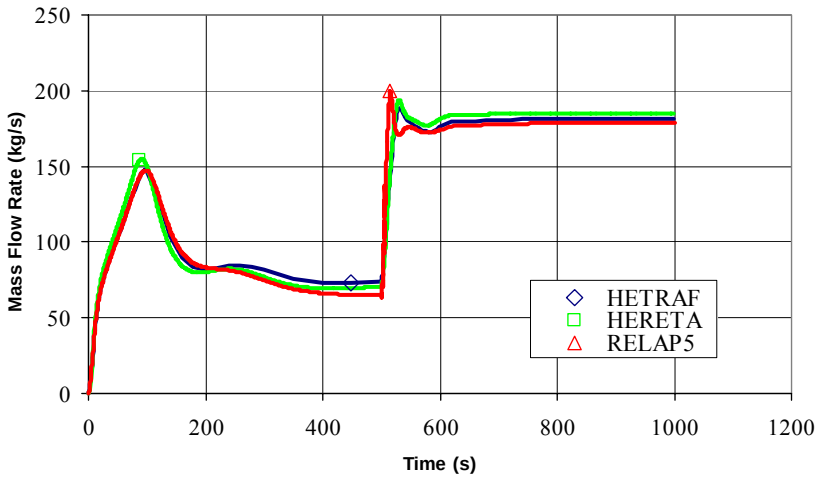


Fig. 6. LBE mass flow rate according to various codes.

Figure 7 presents the maximum LBE temperature in the spallation zone. Again an overall excellent agreement between all three codes is observed. At steady state

conditions, the maximum LBE temperature predicted by RELAP-5 is about 5 °C and 10 °C lower than the values computed by HETRAF and HERETA, respectively.

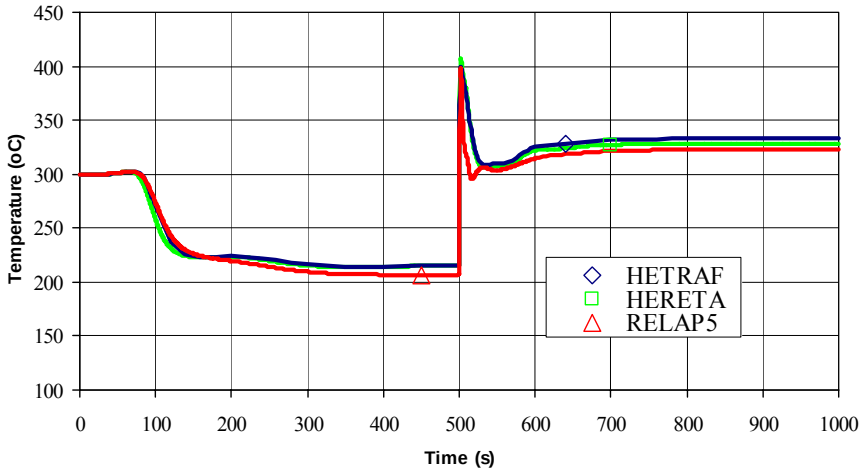


Fig. 7. Maximum LBE temperature according to various codes.

The benchmark shows clearly that all three codes provide similar results. The deviation between HERETA and HETRAF is negligibly small. The minor difference between RELAP-5 and other two codes could be resulted by the discrepancy between physical models and LBE properties used in different codes. Also the introduction of virtual solid material into the spallation zone could be one of the reasons for this minor discrepancy. Due to the high flexibility in user interaction the HERETA code was selected for the subsequent calculations.

### 3.2 System Heat Removal

#### 3.2.1 Steady State & Transient Performance under Beam Start up

The LBE mass flow rate and the LBE temperature at the upper end of the spallation zone are presented in Fig. 8. The transient performance of the XADS target is shown under two kinds of beam start up conditions, i.e., ‘power jump’ and ‘power ramp’. In a start up scenario of power jump, beam power is immediately increased to its full power, whereas a power ramp scenario has a linear increase of beam power. A speed of the increase of beam power depends on a ramp time duration.

At stand-by conditions, an initial LBE mass flow rate of about 72 kg/s is achieved. The temperature peak in case of power jump transient reaches 410 °C. This temperature

peak occurs because the natural circulation flow is not established sufficiently in the early stage of the beam jump. The maximum cross-sectional LBE temperature (i.e., the LBE temperature at the upper end of the spallation zone) at steady state conditions is 335 °C. The LBE mass flow rate is 192 kg/s. It is expected that under the power jump transient, the maximum temperature of the window will far exceed the design limit. Therefore, a beam start up procedure with power jump has to be avoided.

According to the XADS design specification [14], a slow ramp of beam power was defined, i.e., at first a small beam power jump from zero to 45 kW, 1.5 % of the full power, then a linear increase to its full power in a few thousand seconds. To give an impression about the effect of the ramp time duration on the thermal-hydraulic behavior, a transient analysis was carried out with the following start up procedure: at first a beam power jump to 45 kW and then a power ramp to full power in 200 s. In the case of power ramp with a ramp time duration of 200 s, no temperature peak is observed.

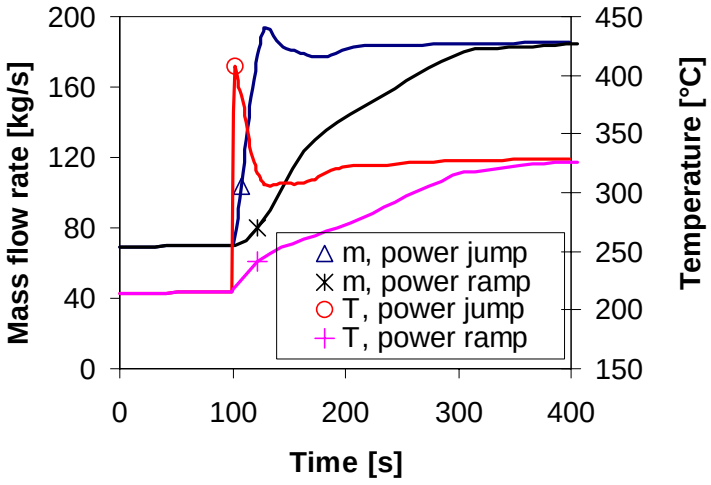


Fig. 8. Transient performance of the target.

3.2.2 Parametric Analysis & Results

*Effect of Funnel Size*

The inner diameter of the funnel is 140 mm in the reference design proposal. This value was taken from the previous concept of ANSALDO. An optimization of the funnel diameter requires a combined analysis of system codes and CFD codes. The CFD results will be described in section 4.3.4. Here, the effect of the funnel size on the overall flow rate and the LBE temperature is investigated. Figure 9 shows the results under beam switch-on transient conditions. The ramp time duration is 200 s. As

recognized, a reduction in the funnel diameter from 140 mm to 120 mm leads to a higher hydraulic resistance, and subsequently, a lower mass flow rate (20 % lower) at steady state conditions. The LBE temperature is about 20°C higher. An increase in the funnel diameter from 140 mm to 160 mm gives about 15 % higher LBE mass flow rate and about 12 °C lower LBE temperature. Due to a larger cross section of the funnel, the average LBE velocity through the funnel is about 7 % lower. This would lead to a reduction in heat transfer. Therefore, final optimization requires CFD analysis.

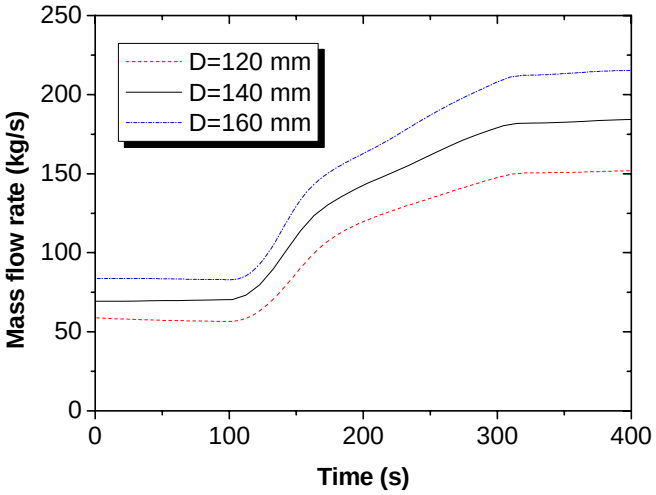


(a) Mass flow rate

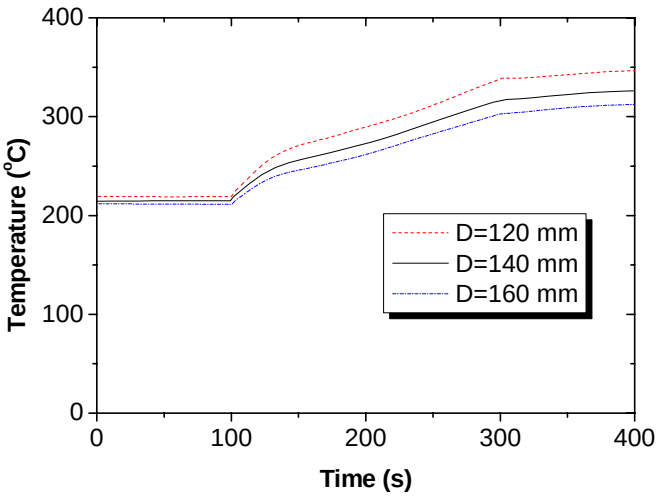


(b) Maximum LBE temperature

Fig. 9. Effects of funnel size.

*Effect of Burnup*

As described in section 2.3, the magnitude of the beam current is increased with fuel burnup. With this variation, the total amount of heat deposition in the target is varied from 1.2 at BOC to 2.4 MW at EOC. Accordingly, the LBE flow rate as well as the LBE temperature is changed. HERETA predicted that the LBE flow rates for BOC and EOC conditions are 149 and 182 kg/s, respectively. The impact on the window temperature will be investigated in section 4.3.5.

*Effect of Conduction through Guide Tube*

In order to investigate the effects of the conduction through the guide tube, one HERETA calculation was performed with the insulated guide tube. It was found that the change of the steady state LBE flow rate is very small. The change of the LBE temperature at the exit of the heat exchanger is also negligibly small. However, the LBE temperature in the spallation zone is decreased by 7~8 $^{o}$C with the insulated guide tube. Therefore, similar amount of the reduction in the window temperature is expected with the insulated guide tube. However, the insulation of the funnel (lower part of the guide tube in the spallation zone) has to be avoided since its temperature will be drastically increased due to heat production in the funnel material.

*Effect of Heat Production Profile*

In the reference case, it is assumed that 80% of spallation heat is released inside the funnel. This portion depends on funnel geometry, proton beam characteristics and also on the interaction between the reactor core and the target. To study the effect of heat deposition profile, an additional case with 100% heat release inside the funnel was analyzed. As shown in Fig. 10, the heat deposition profile does not have any effect on the LBE flow rate and the maximum LBE temperature.

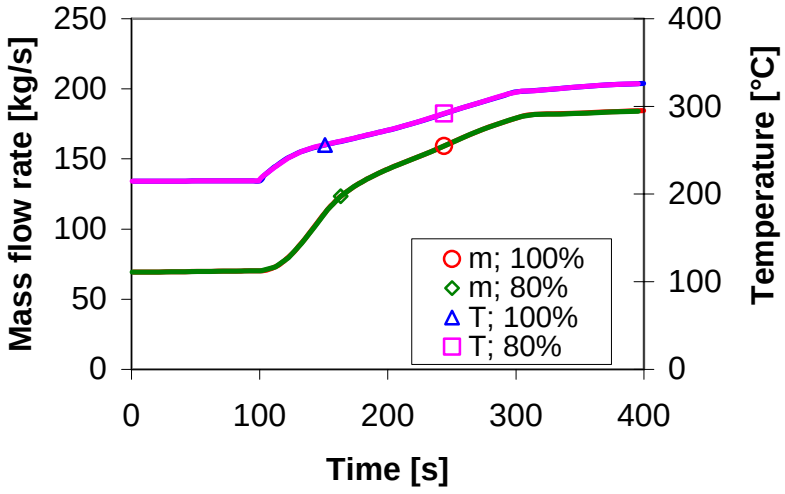


Fig. 10. Effect of heat deposition profile.

### 3.2.3 System Behavior under Beam trip

The operating experience of existing accelerators shows that beam trips occur frequently. Beam trips produce thermal cycle and lead to additional stress, which would become one of the main issues of structural material failure. Improved accelerator performance is required for XADS. Further development of accelerator technology will lead to a reduction in the beam interrupt frequency. In the technical specification of the accelerator for XADS [14], the frequency of beam trips with a time duration longer than 1 second has to be kept below 5 interrupts per year. No special requirements are defined for the beam trips with a beam interrupt duration shorter than 1 second. In order to investigate the effect of such short beam trips, 1D analysis with the HERETA code was performed. The results of HERETA were transferred to CFD analysis in section 4.4.

In order to give a general idea, one of the results of the HERETA calculations is presented here as an example. Figures 11 & 12 show the LBE flow rate and the LBE temperature (at the end of the spallation zone), respectively, in the case of a beam trip with a duration of 0.5 s. It is found that the LBE mass flow rate hardly changes, whereas the LBE temperature drops strongly down from 330 to 260 °C.

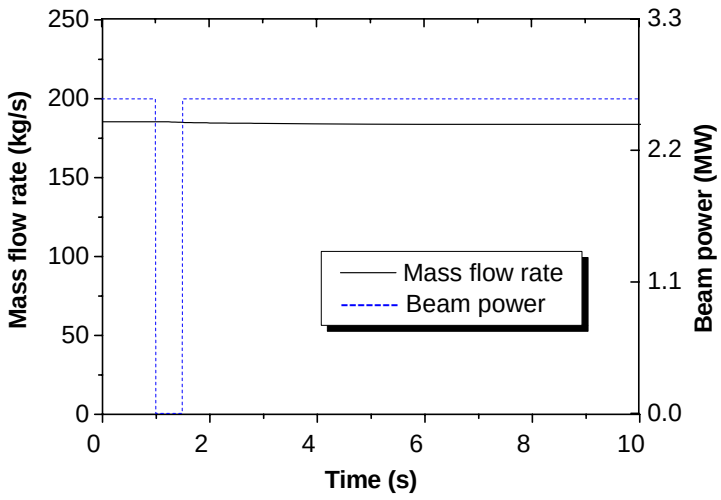


Fig. 11. LBE flow rate under beam trip (0.5 s) conditions.

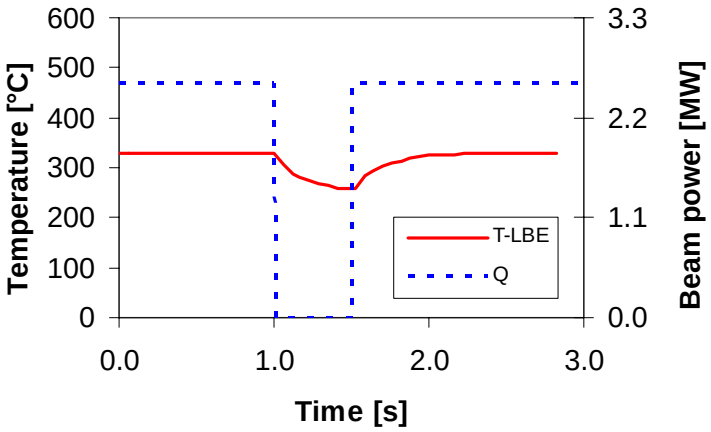


Fig. 12. LBE temperature behavior under beam trip (0.5 s) conditions.

## 4. CFD ANALYSIS OF LOWER PART OF TARGET

### 4.1 Physical Model

For the CFD analysis, the lower part of the target, i.e., from the bottom to an elevation of 1 m above the window, is considered for reasonable computational efforts. Figure 13 shows a schematic view of the lower part of the target with the main geometrical data. The physical description of the target is provided in section 2.1. In the initial stage of the target design the thickness of the window was chosen as 3 mm. One of the challenging issues of the window target is the selection of the window material. In the present work, T91 is chosen as the window material. The thickness of the guide tube is 5 mm. For the guide tube and the beam tube, 316 stainless steel is used. The physical properties used in the CFD analysis are summarized in Tables 2 & 3. The main characteristics of the incoming LBE to the considered domain are listed in Table 4.

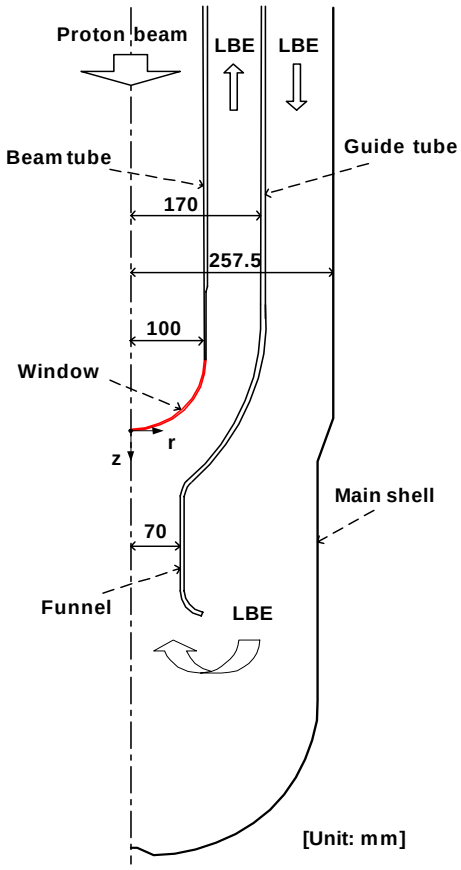


Fig. 13. Schematic view of the lower part of the target.

Table 2. Physical properties of LBE [15]

| Property | LBE (T in $^{o}$C) |
|---|---|
| Density (kg/m$^3$) | 10737 – 1.375 T |
| Thermal conductivity (W/mK) | 7.26+0.0123 T |
| Specific heat (J/kg K) | 146.5 |
| Molecular viscosity (Pa s) | 3.26E-3 – 6.26E-6 T + 4.63E-9 T$^2$ |

Table 3. Physical properties of steels

| Property | 316 steel (T in K) [16] | T91 |
|---|---|---|
| Density (kg/m$^3$) | 8084.2 – 4.2086E-1 T-3.8942E-5 T$^2$ | 7800 |
| Thermal conductivity (W/mK) | 9.248 + 1.571E-2 T | 28.8 |
| Specific heat (J/kg K) | 4200(0.1097 + 3.17E-5 T) | 562.69 |

Table 4. Main characteristics of inlet flow

| Mass flow rate | 192 kg/s |
|---|---|
| Inlet mean velocity | 0.165 m/s |
| Inlet temperature | 233 $^{o}$C |
| Inlet Reynolds number | 213634 |

### 4.2 Numerical Approach

The CFX 5.6 code has been used in this work. It provides the possibility to use various advanced turbulence models combined with an advanced wall treatment, e.g., the Shear Stress Transport (SST) turbulence model with the automatic wall treatment. The adequate selection of the turbulence model on the prediction of the window temperature is very important because flow stagnation occurs just below the window center, where the largest thermal load exists in the window. It was reported in the validation study by Vieser et al. [17] that the SST turbulence model provides better performance than the k-ε and k-ω turbulence models on the prediction of the stagnation heat transfer. The automatic wall treatment is practically useful since it allows the use of coarser meshes near walls than typical low Reynolds number treatments. Therefore, the SST turbulence model with the automatic wall treatment has been applied for the present analysis.

4.2.1 Computational Model

An axi-symmetrical 2D computational domain was chosen due to symmetric conditions. As shown in Fig. 14, the geometry for the computation was generated by revolving a 2D surface with 3 degree. A total of 42 solids were created for structured meshing.

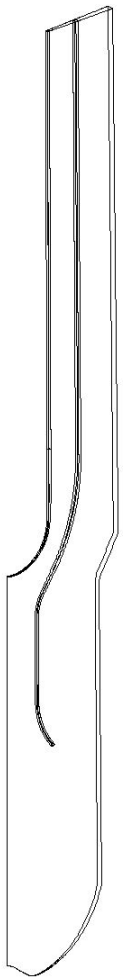

Fig. 14. Computation domain for axi-symmetrical 2D model.

4.2.2 Turbulence & Buoyancy Models

As previously mentioned, the SST turbulence model with the automatic wall treatment in CFX 5.6 was selected. The full buoyancy model available in CFX 5.6 was adopted. For the reference temperature of buoyancy, the average LBE temperature obtained by the prior calculation was applied.

4.2.3 Grid Generation

In the computational domain shown in Fig. 14, hexahedral grids were made except the symmetric axis. In the axis, prisms were placed. One layer of meshes was made for 2D calculations. The total number of grids including prisms is 119012. Fine meshes were applied to regions close to walls, particularly around the window in order that viscous sublayer integration is sufficiently accurate. The computation meshes near the window region are provided in Fig. 15. The size of the first fluid mesh near the window is ~10 μm. In CFD communities, the size of the first fluid mesh is usually represented by $y^+$ (non-dimensional distance from wall). Figure 16 shows the $y^+$ distribution along the outer surface of the window for the reference meshes. A grid sensitivity study confirmed that the grid size used for the present calculations is fine enough.

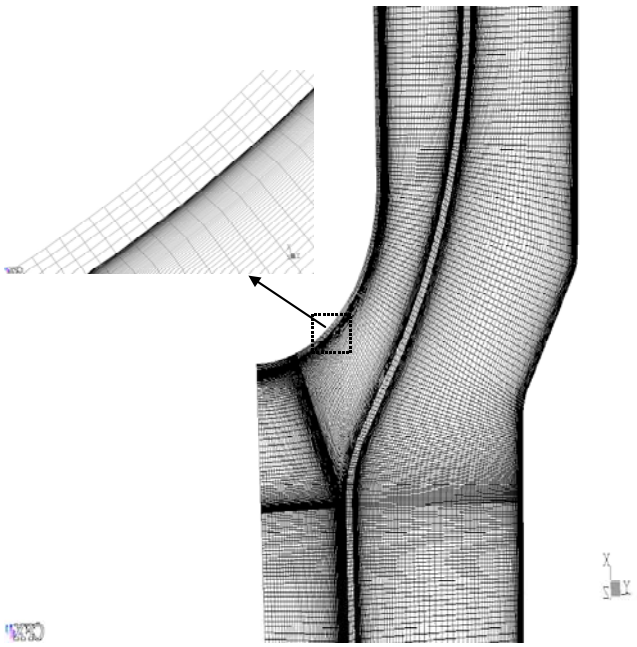

Fig. 15. Computational meshes near the window region.

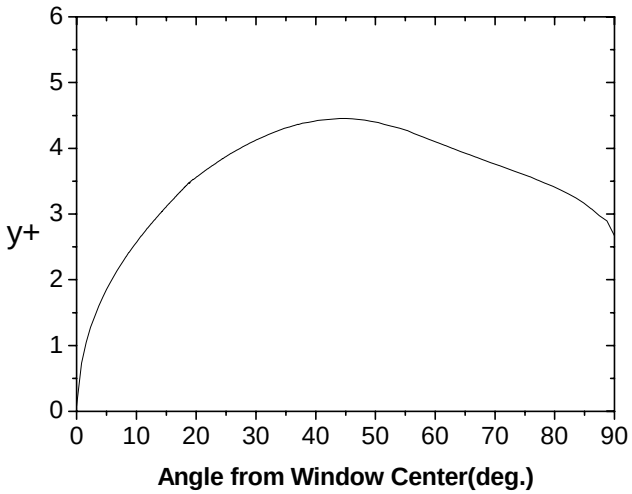


Fig. 16. $y^+$ plot along the outer surface of the window.

### 4.2.4 Spallation Heat Simulation

The spallation heat described in section 2.3 was simulated by user defined heat source for the CFX calculations. The tabulated data file corresponding to the results in [8] was imported to an external user subroutine and a piecewise linear interpolation was made to match the MCNPX meshes with the CFX meshes. Figure 17 shows the simulated spallation heat in CFX 5.6 using the user defined heat source for a beam current of 6 mA. It was carefully confirmed that the deviation of the heat deposition distribution between the data used in CFX 5.6 (Fig. 17) and the original values from the MCNPX calculation (Figs. 3 & 4) is negligibly small. In case of the 3-mm thick window, the maximum heat flux at the window center, where local flow stagnation is expected, can be roughly estimated as 2.7 MW/m$^2$ (=0.9 MW/m$^3$ × 0.003 m). Cooling of the window becomes, therefore, one of the key issues of the target design.

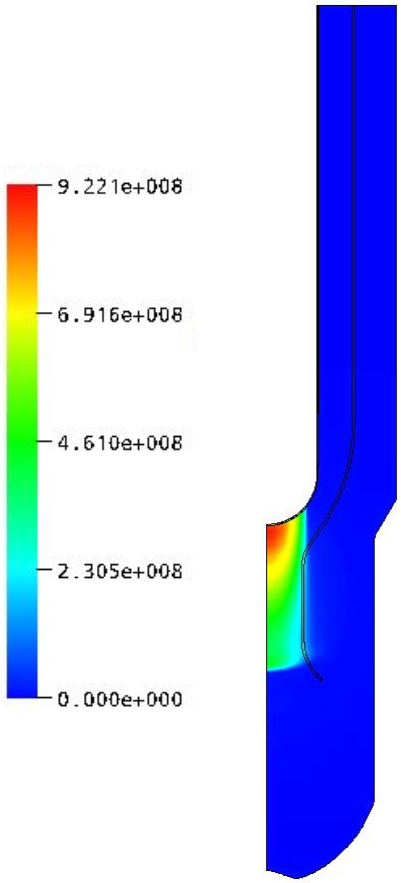


Fig. 17. Simulated spallation heat source in CFX 5.6 (W/m$^3$).

#### 4.2.5 Numerical Scheme

The second order advection scheme was adopted for all the calculations and the second order backward Euler scheme, which is an implicit time stepping scheme with second order accuracy, was applied for transient simulations.

#### 4.2.6 Turbulent Prandtl Number

The default value (=0.9) in CFX 5.6 was used for the turbulent Prandtl number.

#### 4.2.7 Boundary Conditions

Since the target is cooled by natural circulation, thermal hydraulic conditions of incoming flow to the computational domain have to be calculated in advance. These boundary conditions are provided by the system analysis described in section 3. Under steady state conditions, the predicted inlet flow rate and the inlet LBE temperature by the HERETA code are 192 kg/s and 233 $^{o}$C, respectively. Uniform velocity and temperature profiles at the inlet cross section were assumed. For turbulence quantities at the inlet, 5% of the turbulence intensity and the viscosity ratio ($\mu_t/\mu$) of 10, were adopted. These are recommended values in the CFX 5.6 manual [4] when there is no information about the inlet turbulence. It was found by the subsequent sensitivity calculations that the impacts of the inlet turbulence quantities on the velocity and temperature fields are negligibly small. A uniform static pressure was imposed at the outlet cross section.

All external walls, except the main shell (outer target shell) adjacent the reactor core, were considered adiabatic. For the main shell, the temperature profile determined by the HERETA code was applied as fixed temperature boundary conditions. The predicted wall temperature of the main shell by HERETA is in the range of 256 ~ 275 $^{o}$C.

#### 4.2.8 Convergence

The simulations were performed until the maximum residuals of the mass-, momentum-, and energy equations were below the value of $5.0\times10^{-6}$. This value is described in the CFX 5.6 manual as ‘very tight convergence’. The monitoring points at

the center of the window inner and outer surfaces showed that both temperatures converge at the maximum residual of $1.0\times10^{-5}$ under steady-state conditions.

Figure 18 shows the residual plots for the steady state calculation with the 2-mm thick window design. After 814 outer loop iterations, the convergence criterion of the maximum residual of $5.0\times10^{-6}$ was achieved. It took ~12 hours with a Pentium 4 personal computer having 2.66 GHz CPU and 1 GB RAM memory. As shown in Fig. 19, two monitoring points, at the center of the window inner and outer surface, started to be converged after ~200 outer loop iterations.

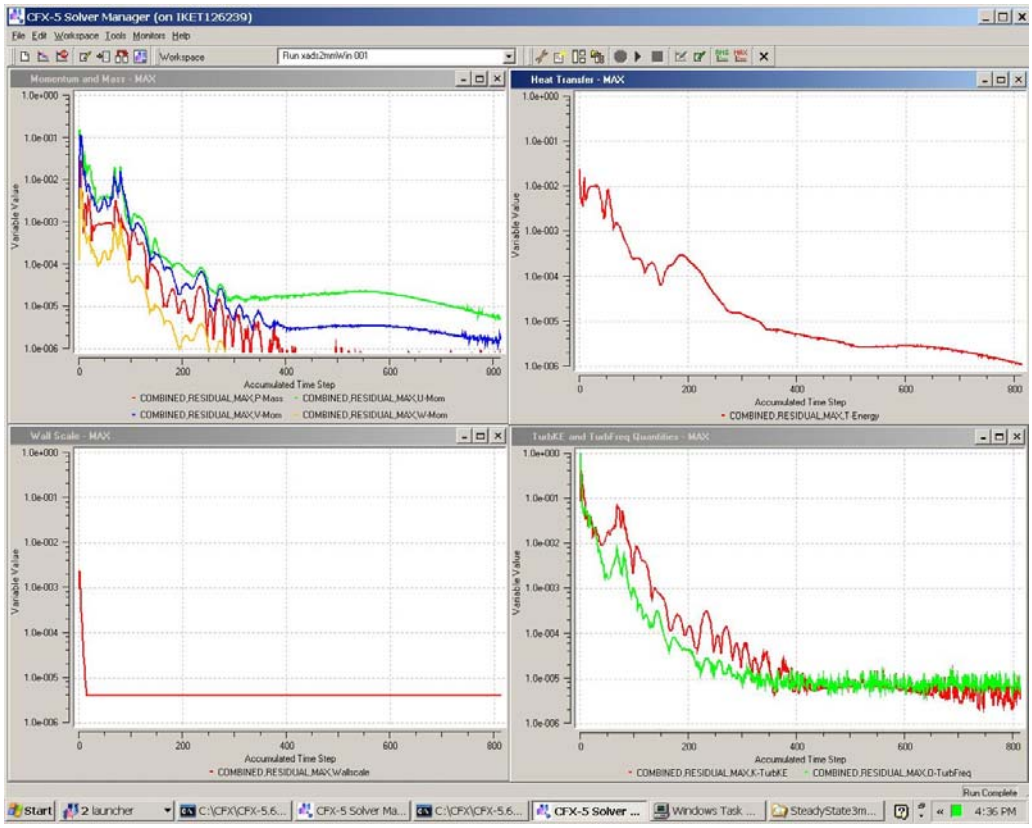


Fig. 18. Typical residual plots for steady state simulation.

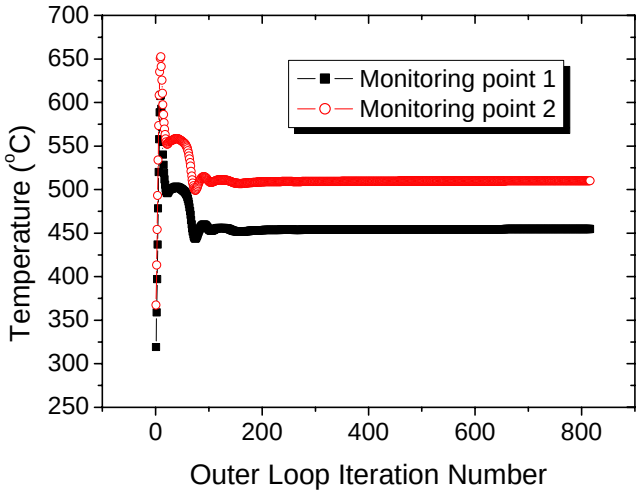


Fig. 19. Behavior of two monitoring points versus iteration number.

### 4.3 Steady State Analysis

#### 4.3.1 Results of Initial Design

At first, a CFX 5.6 calculation was performed for the initial design having a 3-mm thick window. Figure 20 shows the predicted velocity contour in the lower part of the target. As expected, flow stagnation near the center of the window can be seen clearly in Fig. 20. Flow separation occurs both in the downcomer and in the riser. In the downcomer flow separation starts earlier than expected. Additional CFX 5.6 calculation by neglecting the buoyancy effect showed that this earlier separation is caused by the buoyancy effect. The predicted maximum LBE velocity is 1.282 m/s, which is considerably below the design limit 2 m/s.

The corresponding temperature in the lower part of the target and on the window surface is presented in Figs. 21 & 22, respectively. The maximum window temperature occurs in the center of the inner surface and is as high as 596 $^{o}$C. The maximum temperature drop across the window thickness is 123 $^{o}$C. The maximum temperature of the guide tube is 450 $^{o}$C, which is much lower than that of the window. Since the predicted maximum window temperature exceeds the design limit (525 $^{o}$C) significantly, modification of the initial design is inevitable.

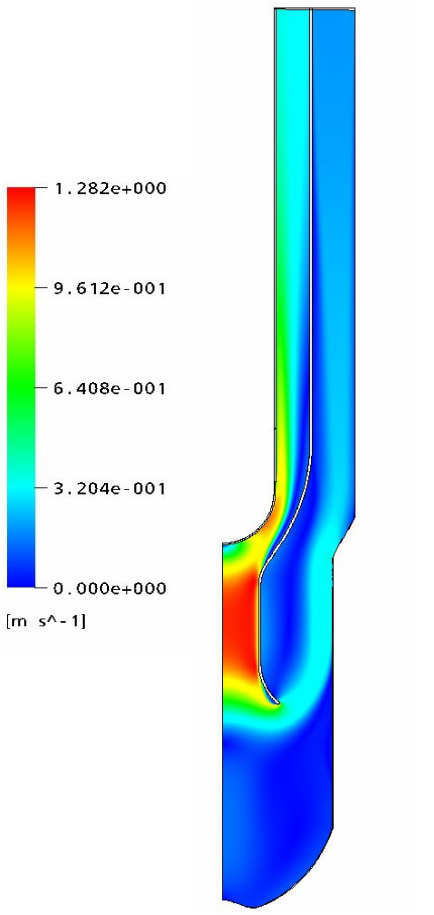


Fig. 20. Velocity contour of initial design (m/s).

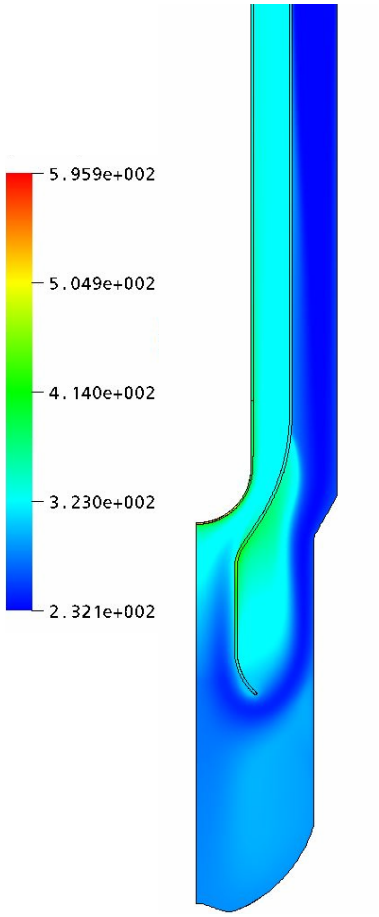


Fig. 21. Temperature contour of initial design ($^{o}$C).

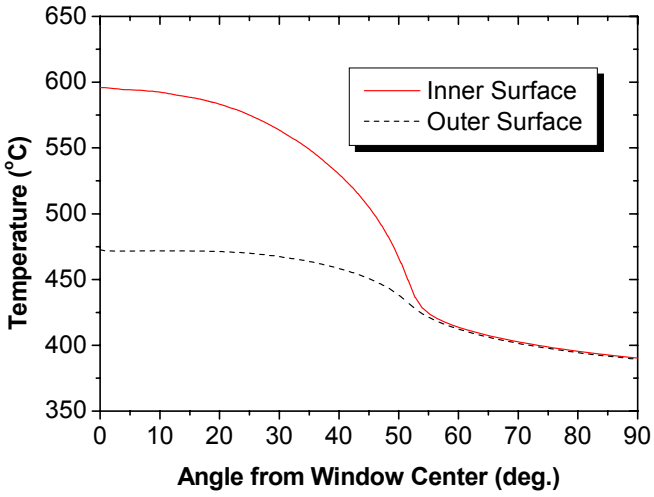


Fig. 22. Window temperature of initial design.

4.3.2 Results of Modified Design

One of the proposals for the modification to the initial design is to reduce the window thickness. Figure 23 shows the CFX 5.6 results with a reduced window thickness. The definition of δ is shown in Fig. 24.

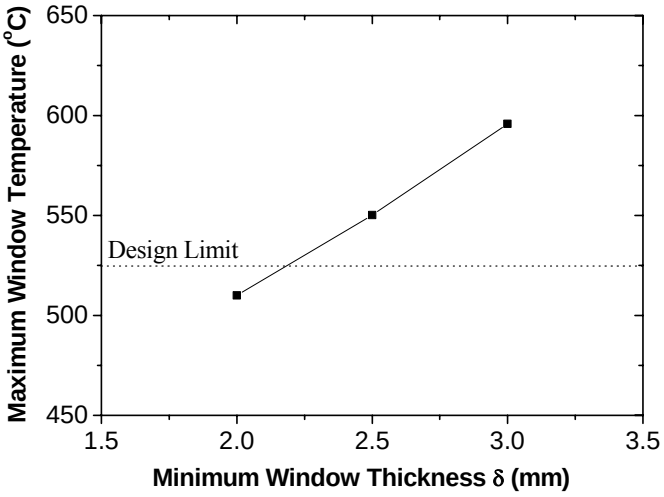


Fig. 23. Effect of window thickness on maximum window temperature.

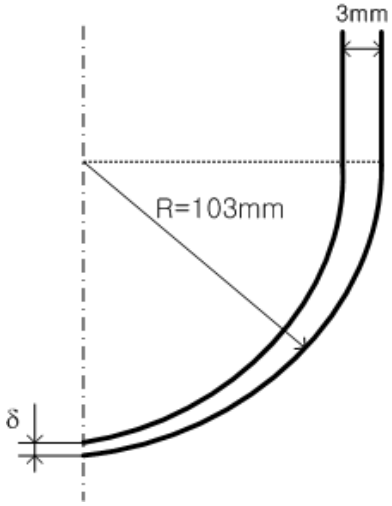


Fig. 24. Definition of δ for window thickness variation.

The window thickness is gradually reduced in the direction to the window center without changing the thickness of the cylindrical part of the beam tube (= 3 mm). By a reduction in the window thickness of 1 mm in the center, the maximum window

temperature is reduced by 86 °C and kept below the design limit. For the 2-mm thick window design, as shown in Fig. 25, the maximum temperature difference across the window thickness is 57 °C, which is smaller than that of the initial design by 66 °C. The structural analysis [18] confirmed that the maximum stress for this modified window design is in the allowable range. Therefore, all the remaining calculations in this report are made for the modified window design with 2 mm thickness in the center.

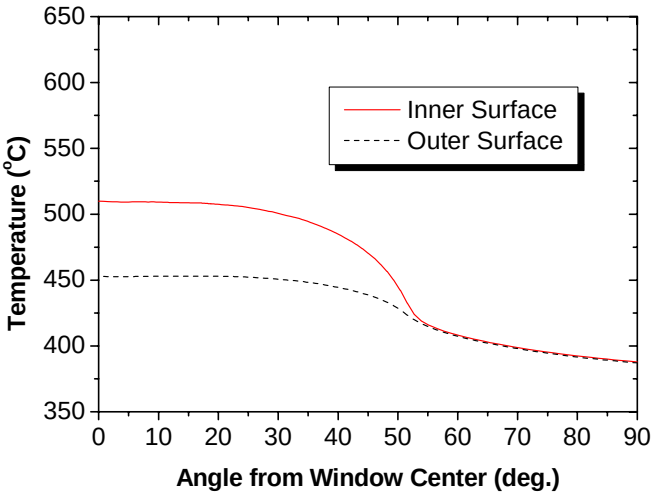


Fig. 25. Window temperature for modified design (2 mm thickness in center).

The maximum temperature of the guide tube is not changed by the modification of the window thickness. It should be noted that the predicted maximum temperature of the guide tube, 450 °C, exactly corresponds to the thermal design limit of the guide tube specified in the technical specification [7].

### 4.3.3 Effects of Structural Material

In order to investigate the effects of structural material, the additional HERETA and CFX 5.6 calculations were performed with the assumption that all structural materials in the target unit (the window, the beam tube, the guide tube, the main shell, the heat exchanger tubes) are made of T91. The conductivity of T91 is larger than that of 316 stainless steel by ~50%.

Due to the increased heat transfer in the heat exchanger, the LBE temperature at the exit of the heat exchanger is reduced by 3 °C but the change of the LBE flow rate is

very small. It is increased by 0.16 %. The LBE temperature at the inlet of the CFX computational domain and the wall temperature of the lower part of the main shell are reduced by about 3 $^{o}$C. The maximum window temperature is reduced by 2 $^{o}$C. However, the maximum temperature of the guide tube is reduced by 14 $^{o}$C. The change of the temperature of the guide tube is much larger than that of the window because the material of the window is not changed. Due to the heat production in the guide tube, the temperature of the guide tube is sensitive to its conductivity. Therefore, the use of a better conductive material for the guide tube (especially the funnel) can be a solution to reduce the maximum temperature of the guide tube.

### 4.3.4 Effects of Funnel Size

A series of HERETA calculations showed that the size of the funnel is an important design parameter affecting the natural circulation flow around the target. (See section 3.2.2.) As shown in Fig. 26, in case of a wider funnel, the LBE flow rate is increased due to relatively small flow resistance. But the injection speed to the window is decreased due to the increase in the flow area. Both effects contribute oppositely to the window cooling. Therefore, detailed simulations are necessary to get an optimum size of the funnel.

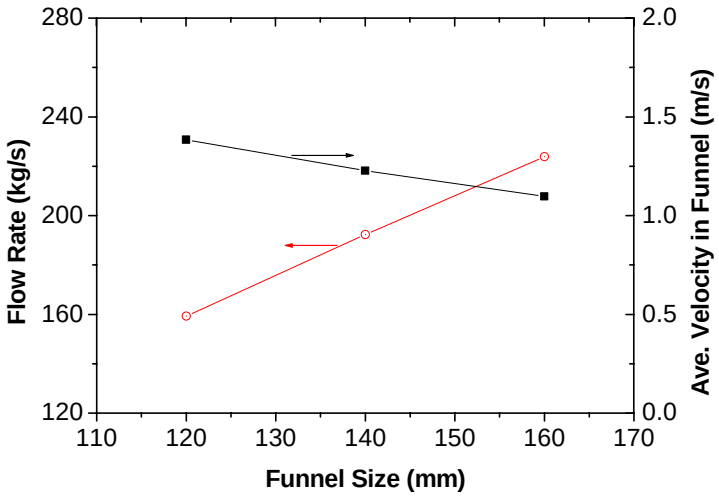


Fig. 26. Effects of funnel size on mass flow rate and average LBE speed in funnel.

Figure 27 shows the results of the CFX 5.6 calculations for three funnel sizes. When the funnel size is reduced by 20 mm from the reference funnel size (=140 mm),

the maximum window temperature is reduced by 7 °C. However, the temperature of the guide tube increases dramatically, because the heat generation rate in the guide tube is larger than that of the original design. Furthermore, it is deduced from a sensitivity study that a reduction in the guide tube thickness can not reduce the maximum guide tube temperature down to the design limit. When the funnel size is increased by 20 mm, the maximum window temperature is increased by 21 °C, and exceeds the design limit. Based on the above results, the reference funnel size is, therefore, considered as the optimum value from the thermal hydraulic point of view.

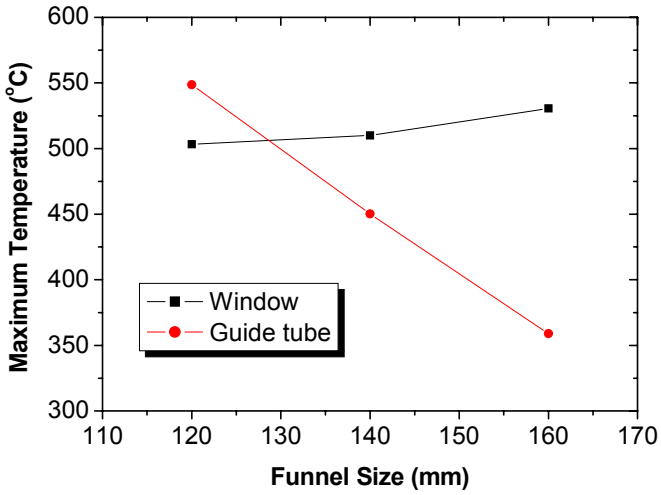


Fig. 27. Effects of funnel size on maximum temperatures of window and guide tube.

4.3.5 Effects of Burnup

As described in section 2.3, the beam intensity, and subsequently the spallation heat, is varied with the fuel burnup. This drives the change of the steady state LBE flow rate from 149 kg/s at BOC to 183 kg/s at EOC, as described in section 3.2.2. The HERETA code also predicted that the inlet temperature of LBE is changed from 214 °C to 228 °C.

Certainly, the window temperature also varies with the fuel burnup. Based on the predicted boundary conditions by the HERETA code, CFX 5.6 calculations were performed for both BOC and EOC conditions and the results are shown in Fig. 28. It can be seen that the maximum window temperature is far below the design limit during the entire fuel cycle (~ 3 years).

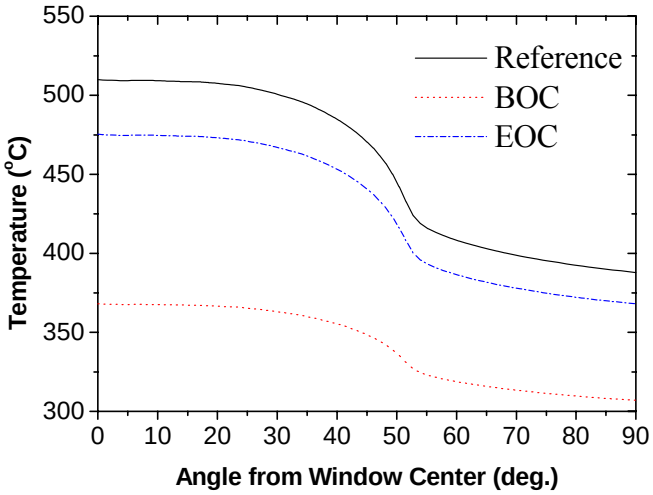


Fig. 28. Temperature profile of inner surface of window in BOC and EOC conditions.

### 4.4 Transient Analysis for Beam trip

This analysis focuses on beam trips with an interrupt duration shorter than 1 second. The frequency of beam trips with an interrupt duration longer than 1 second is limited by 5 times per year in the technical specification of the XADS accelerator [14]. No special requirements are defined for the beam trips with an interrupt duration shorter than 1 second.

Beam trips with four different interrupt durations, i.e. 0.1, 0.3, 0.5, and 1 second, were investigated. As described in section 3.2.3, the HERETA calculation showed that the mass flow rate of LBE and the inlet LBE temperature are hardly changed during beam trips with a short interrupt duration. In case of the beam trip of 1 s, the change of the mass flow rate of LBE is less than 2% and the change of the LBE exit temperature from the heat exchanger is less than 1 $^{o}$C. CFX 5.6 calculations were performed to investigate in detail the behaviour of the window temperature under various beam trip conditions.

Figure 29 presents the predicted temperatures at the central point of the inner and outer surface of the window. For better understanding, the case of beam shut off was also simulated and presented in Fig. 29. In Fig. 29, the beam interrupt starts at the time point 0 s, and the beam power recovers after the corresponding trip periods, i.e., beam interrupt duration. The temperature drop and the temperature recovery in the window can be seen clearly in Fig. 29. As expected, beam trips with a smaller trip period result

in a smaller temperature drop. The window undergoes a temperature drop up to 207 $^{o}$C for the trip period of 1 s, whereas the maximum temperature drop is only 32 $^{o}$C for the trip period of 0.1 s.

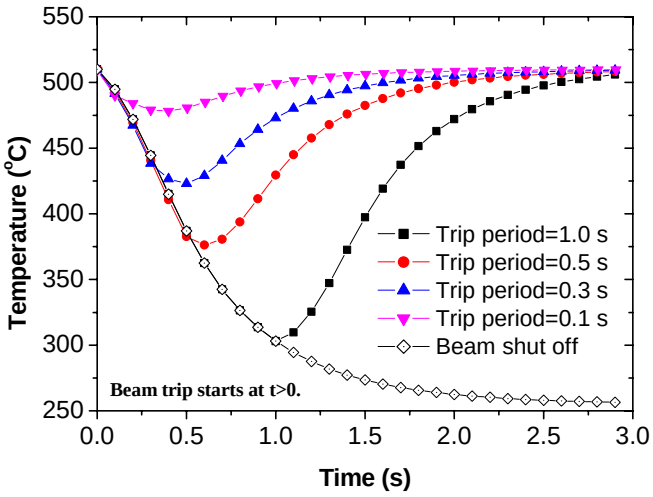


(a) Center of inner surface of the window

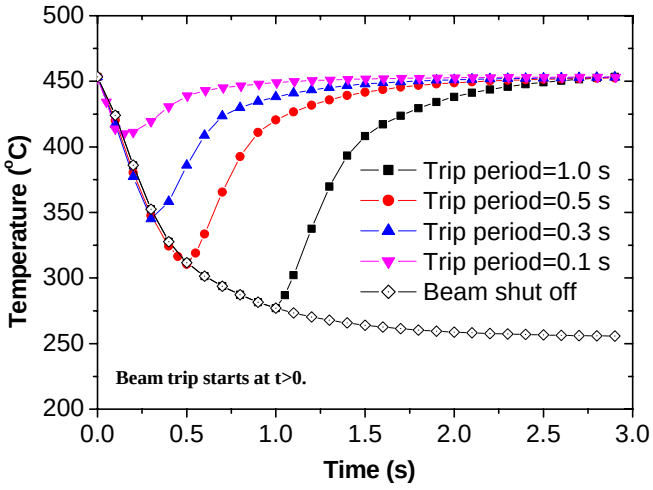


(b) Center of outer surface of the window

Fig. 29. Temperature behaviors under investigated beam trips.

Figure 29 also shows that the steepest slope is located between 0 and 0.5 s after the beam interrupt, regardless of the investigated interrupt duration. Therefore, additional CFX 5.6 calculations were performed with a much finer time step for the first 0.5 s after the beam interrupt, in order to evaluate the maximum temperature change rate more accurately. The result is presented in Fig. 30. The predicted maximum temperature change rate is as high as 412 $^{o}$C/s, at the center of the outer surface of the window. This maximum temperature change rate occurs at 0.1 s after the beam interrupt.

It is clear that beam trips with a trip period shorter than 1 s could also be crucial event affecting the integrity of the window although no attention was paid to these trips in the technical specification of the XADS accelerator. Moreover, it is expected that beam trips with a trip period shorter than 0.1 s do not have enough time to reach the maximum temperature change rate of 412 $^{o}$C/s. It is thus concluded that related to both the maximum temperature drop and the temperature change rate, beam trips with a trip period shorter than 0.1 s are less critical than those with a trip period longer than 0.1 s, and are not further analyzed in this work. Furthermore, it shows that the numerical time step for the CFX calculation has to be much smaller than 0.1 s, to catch accurately the behavior of the temperature change rate.

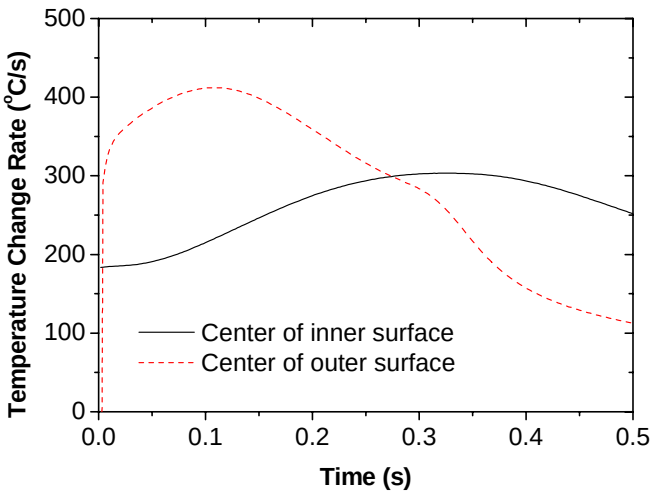


Fig. 30. Window temperature change rate after beam interrupt.

## 4.5 Safety Analysis

Three kinds of abnormal accidents (i.e., beam focusing, loss of heat sink, and unexpected beam jump) were analyzed in the present work regarding the safety analysis of the XADS spallation target. The main concern of the present accident analysis is to know how quickly the beam has to be switched off to avoid window failure. There are two important time points related with the integrity of the window. The first one is the time when plastic deformation of the window starts. For example, plastic deformation of the window in the MEGAPIE target is not allowed [19]. The second one is the time of window failure. Although the melting temperature of T91 is far above 1000 $^{o}$C, it is clear that window failure occurs before its melting point because the window is under both mechanical and thermal stresses. The results of the tensile test of fresh T91 [20] and the stress analysis [18] indicate that the window could fail at about 700 $^{o}$C under the stress in normal operation conditions. More data under irradiation with LBE environment are required for a more accurate prediction of window failure. In the present work, however, 700 $^{o}$C is used as a rough estimation for the temperature, at which window failure occurs.

### 4.5.1 Beam Focusing

In order to expand the proton beam onto the target, two approaches are available in principle. The technique used by the MEGAPIE target involves defocusing the beam by means of additional quadrupoles. The other approach is to apply the so-called raster scanning method deflecting a pencil-like beam with fast magnets in a designed pattern to paint the target area. The reference accelerator for XADS uses the second method. Therefore, a focused beam accident is caused by failure of rastering magnets. There are 4 rastering magnets for beam scanning in the XADS accelerator and one pair of magnets covers each axis of the footprint of the beam (i.e., circle with a radius of 8 cm). Therefore, if one of the rastering magnets fails, the proton beam will cover only the half of the entire footprint with the same beam power. It means the beam intensity becomes double for one half of the target in case of one rastering magnet failure.

An accident initiated by one rastering magnet failure was simulated by the CFX 5.6 code using the doubled beam current (=12 mA). To simplify the analysis, the computational model and boundary conditions used for the reference steady state analysis were unchanged except the beam current. These assumptions (in particular, axi-symmetrical 2D assumption) are not realistic, but they provide conservative results. Figure 31 shows the result of CFX 5.6. It can be seen that the maximum window temperature arrives at 700 $^{o}$C in 0.8 second after the failure of one magnet. The window failure will occur even at an earlier time point since the thermal stress is increased with

the doubled beam intensity. The result of the tensile test indicates that the window will not fail in the first 0.1 second, because the maximum window temperature is lower than 550 $^{o}$C. Therefore, it can be said that the window failure will occur during 0.1~0.8 second after the failure of one rastering magnet.

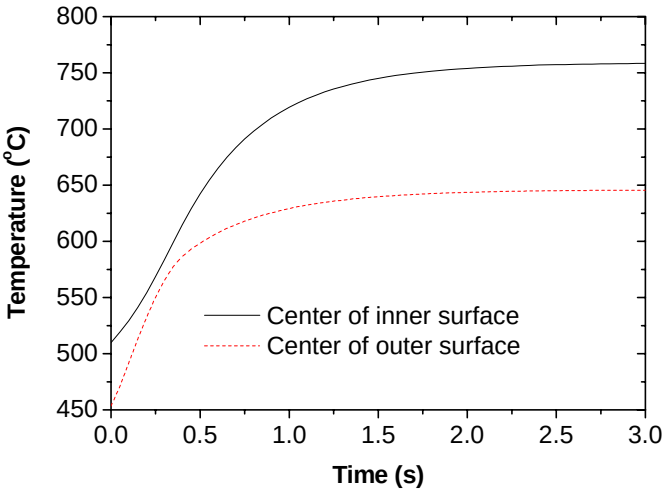


Fig. 31. Window temperature behavior under doubled proton beam current.

4.5.2 Loss of Heat Sink

Under normal operation conditions, the spallation heat is transferred to the secondary oil loop through the heat exchanger in the target module. The oil loop itself is also cooled by another cooling loop. Therefore a loss of heat sink accident is a probable event in the XADS spallation target. It could happen when either of the cooling loops is inactive. In the present work, the worst event, i.e., complete loss of heat sink, has been considered.

Figure 32 shows the mass flow rate and the LBE temperature at the exit of the heat exchanger under a complete loss of heat sink case. The LBE flow rate is slowly reduced. It is still kept 78 % of the initial value after 400 seconds. However, the LBE temperature at the exit of the heat exchanger is sharply increased after the loss of heat sink. Figure 32 also shows that the window failure will occur before 400 seconds, because the window temperature is always much higher than the LBE temperature at the exit of the heat exchanger. For more detailed window temperature, CFX 5.6 calculations were performed. Since the flow transient is not rapid, steady-state assumption was made and the CFX analysis was carried out for three time points (=100, 200, 300 seconds)

based on the boundary conditions supplied by HERETA. Figure 33 shows the maximum window temperature at 100, 200, and 300 seconds after the start of heat sink loss. It can be seen that the window failure occurs at ~200 seconds.

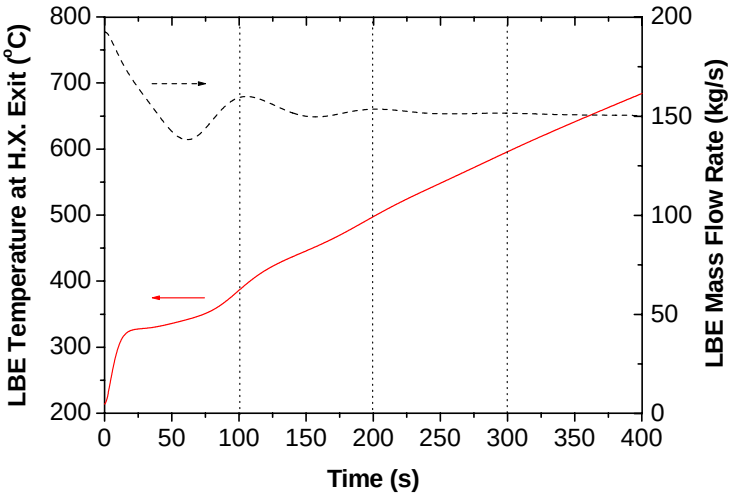


Fig. 32. HERETA results under loss of heat sink accident.

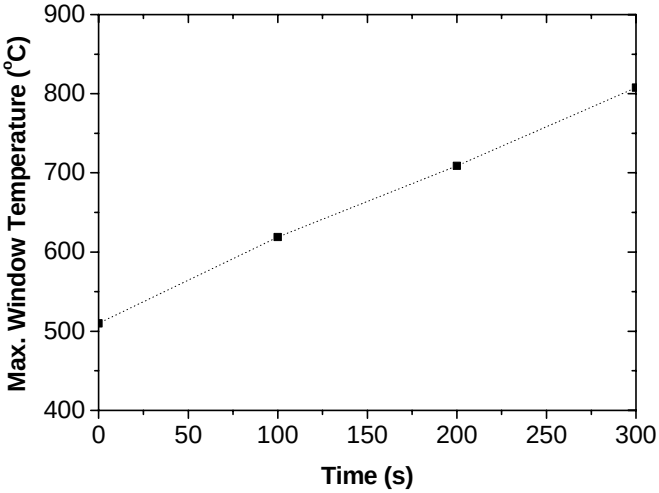


Fig. 33. Maximum window temperature vs. time under loss of heat sink accident.

4.5.3 Unexpected Beam Jump

As shown in Fig. 8, sudden beam jump causes temperature peak in the target and may damage the window. Therefore, it is worth while to investigate the window temperature for such events. Results of beam jump events very depend on the time when beam jumps occur. If a beam jump occurs before heat exchanger operation, the result from the event would be the most severe. However, it is the least probable. More probable beam jump occurs during normal operation period with full reactor power. Figure 34 shows the mass flow rate and the LBE temperature at the exit of the heat exchanger when the beam current is suddenly increased from 3 to 6 mA. The mass flow rate reaches a small peak after ~25 seconds and stabilizes to the steady-state value. It never drops down below the initial flow rate. The LBE temperature at the exit of the heat exchanger is increased by ~20 $^{o}$C.

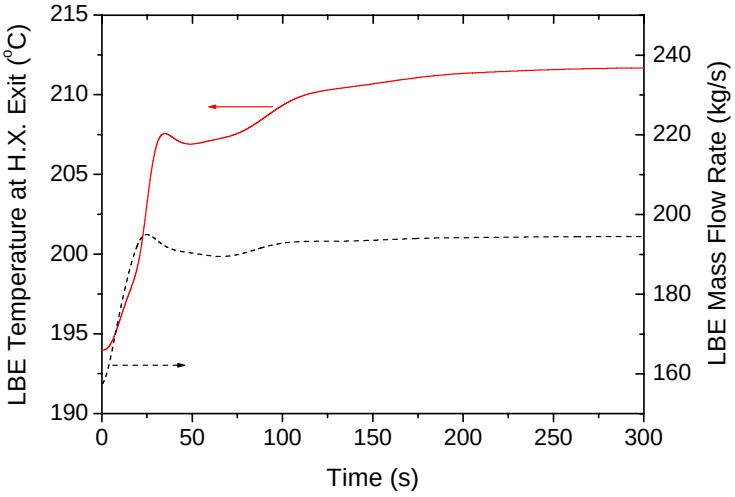


Fig. 34. HERETA results under a beam jump from 3 to 6 mA.

In order to minimize the computing load, one steady-state calculation was performed using CFX 5.6 with the most conservative assumptions to investigate the window temperature under a beam jump during normal operation conditions with full reactor power. For a conservative calculation, the cooling conditions are kept to BOC conditions but the beam current is changed from 2.47 to 6 mA. With these assumptions, CFX 5.6 predicted the maximum window temperature as high as 550 $^{o}$C only. Therefore, window failure is not expected for beam jump events during normal operating period with full reactor power.

## 5. CONCLUSIONS

Among the proposed spallation target designs in the PDS-XADS project, the window target unit for the LBE cooled primary core is considered as one of the basic options for XADS. In the present work, thermal hydraulic analysis has been performed for this option focusing on the cooling capability of the window. Based on the results of HERETA and CFX 5.6 calculations, the following conclusions are made:

- At steady state conditions, a stable natural circulation flow is established with a LBE flow rate of 192 kg/s. No temperature peak is observed by a start up procedure with a beam ramp having a period of 200 s.
- A start up procedure with beam jump has to be avoided to prevent the overheating of the window.
- During a beam trip shorter than 1 s, the change of the LBE flow rate is negligibly small.
- The maximum steady state temperature of the initially proposed 3-mm thick window exceeds the design limit by 71 $^{o}$C for the reference condition of 6 mA beam current.
- By a reduction in the thickness of 1 mm in the center, the maximum window temperature is reduced to 510 $^{o}$C and is kept below the design limit.
- The reference funnel size (=140 mm) is proven as an optimum value in terms of the cooling capability of the window and the guide tube.
- During the entire fuel cycle (~ 3 years) the maximum window temperature for the modified design (2-mm thick window in center) is far below the design limit.
- The temperature drop under the beam trip of 1 s trip period is predicted up to 207 $^{o}$C. Beam trips with smaller trip periods result in smaller temperature drops.
- For all beam trip conditions analyzed, the predicted maximum temperature change rate is as high as 412 $^{o}$C/s, which occurs about 0.1 s after the beam interrupt.
- Beam trips with a trip period less than 1 second could also be crucial events affecting the integrity of the window, and, therefore, need to be considered in the design of the XADS accelerator.
- In case of beam focusing, window failure occurs about 0.1 ~ 0.8 second after the start of the rastering magnet failure.
- For a loss of heat sink accident, the predicted time for a window failure is about 200 s.
- Window failure is not expected for a beam jump event during normal operation period with full reactor power.

Nowadays, due to the fast development of computer hardware as well as software, more and more applications of CFD codes to nuclear engineering and designs are envisaged. Although a CFD code is believed to be the best tool for the design and analysis of spallation targets, it should be noted that the validation of CFD codes is still not completed in particular areas such as turbulent heat transfer in liquid metals.

**Acknowledgements**

This study was carried out in the framework of the PDS-XADS project partially financed by the 5th Framework Programme of the European Commission (Contract number FIKW-CT2001-00179).

## References


[1] A European Roadmap for Developing Accelerator-Driven Systems (ADS) for Nuclear Waste Incineration, Report of the European Technical Working Group on ADS, April, 2001.

[2] B. Carluec, The European project PDS-XADS - "Preliminary Design Studies of an eXperimental Accelerator-Driven System", Proceedings of the Intern. Workshop on P&T and ADS Development 2003, Mol, Belgium, October 6-8, 2003. SCK-CEN Belgian Nuclear Research Center, Mol, 2003 CD-ROM, BLG-959

[3] D. Coors et al., Target Units for XADS Primary System, EURADWASTE 04, Luxembourg, March 29-31, 2004.

[4] CFX 5.6 Manuals, ANSYS Incorporated, 2003.

[5] A. Batta et al., "Window Target Unit for the XADS Lead-bismuth Cooled Primary System", Proceedings of the International Workshop on P&T and ADS Development 2003, Mol, Belgium, October 6-8, 2003. SCK-CEN Belgian Nuclear Research Center, Mol, 2003 CD-ROM, BLG-959

[6] X. Cheng et al., Design Analysis of the Spallation Target for the European Experimental ADS, AccApp '03, San Diego, U.S.A, June 1-5, 2003.

[7] L. Cinotti et al., Technical Specification and Target Unit Interface (LBE and gas cooled concept, window and windowless options), Report-No. XADS 43 TIIX 010, Ansaldo Nucleare, July, 2002.

[8] C.H.M. Broeders, Physics Investigations for the Spallation Target of the LBE-cooled Window Option XADS Design, DOC04/335, April 2004.

[9] H.-J. Neitzel, J.U. Knebel, Auslegung eines geschlossenen 4 MW-Targetmoduls mit Wärmeabfuhrsystem für eine ADS-Anordnung, Forschungszentrum Karlsruhe, Report-No. FZKA 6687, February, 2002.

[10] X. Cheng, Numerical Analysis of Thermally Induced Transients in Forced Flow of Supercritical Helium, Cryogenics, Vol.34, No.3, p.195-201, 1994.

[11] J.U. Knebel, X. Cheng, N.I. Tak, Thermalhydraulic Design of the MEGAPIE Spallation Target, 5$^{th}$ Topical Meeting on Nuclear Applications of Accelerator Technology, Reno, November 11-16, 2001.

[12] Ansaldo, RELAP5/Mod3.2.2 Beta Release, Private Communication, April 15$^{th}$, 2003.

[13] P. Coddington et al., Safety Analysis of the EU-PDS-XADS Designs, OECD/NEA Fourth International Workshop on Utilization and Reliability of High Power Proton Accelerators, Daejeon, Korea, May 16-19, 2004.

[14] P. Richard et al., Technical Specifications, Missions of XADS, Recommendations for the Main Characteristics, DER/SERI/LCSI-02/4002, CEA, July 2002.

[15] S. Cevolani, Review of the Liquid Lead-Bismuth Alloy Physical Properties, ENEA Report, DT.SBD.0004, April 1998.

[16] Y. S. Tang et al., Thermal Analysis of Liquid-Metal Fast Breeder Reactors, American Nuclear Society, 1978.
[17] W. Vieser et al., Heat Transfer Predictions using Advanced Two Equation Turbulence Models, CFX Technical Memorandum, CFX-VAL10/0602, 2002.
[18] A. Zucchni and P. Turroni, Target Unit-Thermal-Mechanical Analysis in Normal and Off-normal Conditions (LBE Primary System Concept, Proton Beam Window Option), June 2004.
[19] B. Smith, Private Communications, March 2004.
[20] F. Groeschel, Private Communications, March 2004.